ASSESSMENT OF A FUEL CELL POWERED FULL ELECTRIC SUBSYSTEM ARCHITECTURE FOR THE AVACON RESEARCH BASELINE AIRCRAFT

Jasper van Wensveen[1], Fabian Peter[1], Tobias Rau, Mirko Hornung[1]

[1]Bauhaus Luftfahrt e.V., Willy-Messerschmitt-Straße 1, 82024 Taufkirchen, Germany

ABSTRACT

This paper presents work from the research project AVACON on subsystem design and analysis: a first potential assessment of a polymer electrolyte membrane fuel cell powering a full electric subsystem architecture and replacing the conventional auxiliary power unit. The electrical subsystems power load calculations and the component sizing of the fuel cell system are performed with a mix of statistical, semi-empirical, and semi-analytical methods within the tool eFLOWpy. A 2% operational empty mass increase is assumed to account for the subsystem electrification mass change. The fuel cell system considered consists of six fuel cell stacks, a liquid hydrogen storage tank, a compressor to provide cabin air and a cooling loop with heat exchanger. The mass and volume of the fuel cell system is calculated on a main component basis. The overall sizing and analysis considers a standard mission trajectory including diversion. The results show a kerosene block fuel reduction of 1.2% compared to the AVACON research baseline aircraft with conventional subsystems, while further fuel cell system optimisation could potentially lead to a 3% reduction.

NOMENCLATURE

ASR	Area-Specific Ohmic Resistance	FCS	Flight Control System
APD	Aircraft Preliminary Design - commercial software	HHV	Higher Heating Value
APU	Auxiliary Power Unit	ISA	International Standard Atmosphere
ARB	AVACON Research Baseline	MHX	Main Heat eXchanger
CAC	Cabin Air Compressor	MTOM	Maximum Take-Off Mass
ECS	Environmental Control System	OEM	Operational Empty Mass
ELA	Electrical Load Analysis	PE	Power Electronics
EM	Electric Motor	PEM	Polymer Electrolyte Membrane

1. INTRODUCTION

The advances in electrified aircraft subsystems offer the potential of fuel savings, amongst other benefits like reduced maintenance efforts. Reducing or removing the bleed air off-takes from the engines improves their specific fuel consumption, while electrification of the subsystems results in a mass change. The net effect of full subsystem electrification on fuel consumption is generally considered positive. Chakraborty, for example, estimates a block fuel saving of 3.1 to 4.0% depending on the aircraft size [1]. Similar saving magnitudes ranging from 1.6% to 4.8% can be found in other sources [2–6]. These configurations, however, still use electrical power off-takes through generators installed on the engines. Generating the required power through an alternative energy source (e.g. a fuel cell system) and removing the electrical engine off-takes may allow further improvement of the specific fuel consumption. Hence, a trade-off between mass and specific fuel consumption arises. On the other hand, the aircraft subsystems have a large influence on the overall aircraft design, and certification of subsystems is cost intensive, which makes them difficult to retrofit. It is therefore important to assess possible subsystem architectures during the conceptual aircraft design phase.

Funded by the German national aeronautic research program, the research project AVACON (**AdV**anced **A**ircraft **CON**cepts) aims at collaborative design and technology assessment for future aircraft. Nine different partners from the industry, research entities and universities work together on different disciplines. A research baseline aircraft, sized for the middle of the market, serves as starting point for the various technology and configuration assessments. Bauhaus Luftfahrt, together with Hamburg University of Technology, is responsible for designing and analysing subsystem architecture possibilities within the project. This paper presents the work performed for a first potential assessment of a full electric subsystem architecture powered by a Polymer Electrolyte Membrane (PEM) fuel cell for the AVACON Research Baseline (ARB) aircraft. Table 1

presents the top-level aircraft parameters of this aircraft.

Table 1: Overview of the AVACON research baseline aircraft top-level aircraft requirements.

Top-level aircraft requirement	Value	Unit
Maximum take-off mass	140	t
Passengers	252	-
Wing Span	52	m
Cruise Mach number	0.83	-
Design range	4600	NM
Entry-into-service	2028	-

2. METHODOLOGY

In 2018, development of the in-house tool eFLOWpy started to support conceptual aircraft design work at Bauhaus Luftfahrt. Currently eFLOWpy allows the modelling and assessment of hybrid-electric powertrains, as well as conventional and electrical subsystem architectures on different levels of detail. While the two disciplines are currently still separate parts within the tool, full integration is planned on the long term. The work described in this paper added PEM fuel cell system sizing and analysis capabilities to eFLOWpy. Section 2.1 will elaborate on the subsystems part of eFLOWpy in more detail, while section 2.2 describes the fuel cell modelling part.

2.1. Subsystems modelling

The subsystems part of eFLOWpy has a modular and multi-fidelity setup. Each subsystem to be analysed has its own top-level ATA chapter. The user is free to create and add additional ATA subchapters and/or custom components underneath the main ATA chapters. Figure 1 provides an example schema of this. Internally, the subchapters are simply components themselves as well, and each component may have a collection of sub-components assigned to it (where these subcomponents are in fact of the class component themselves again). Each ATA chapter and component can have its own mass and power model assigned to it and the user is free to create new models or use pre-existing models. The tool starts to size and analyse the lowest tier components, combines the mass properties and power characteristics, and propagate them upwards to the next level. If a component has models assigned while also having subcomponents, the results of these models are added as 'overhead' values. Ultimately, all the component results together form the total mass properties and power characteristics per ATA chapter.

In order to save time and effort, the AVACON study presented here does not consider mass property modelling of the subsystems. Instead a 2% Operational Empty Mass (OEM) increase, based on the results of Chakraborty [1], is used to account for the mass change due to subsystem electrification. The power characteristics are calculated on ATA chapter level. Table 2 provides an overview of the ATA chapters considered and their respective power models. The power models used are a mix of statistical, semi-empirical, and semi-analytical methods. The ATA chapters that do not have a significant influence on the total power consumption are modelled by scaling the loads provided in the Electrical Load Analysis (ELA) of an existing and representative passenger aircraft. These loads, defined per mission segment, represent the maximum expectable load during normal operations. The remainder of this section will describe the power model of ATA21 air conditioning and ATA27 flight controls in more detail, as they are larger power consumers.

2.1.1. ATA21 air conditioning

The model used to calculate the Environmental Control System (ECS) power demand uses a cabin heat balance approach. The power loads of ATA22,
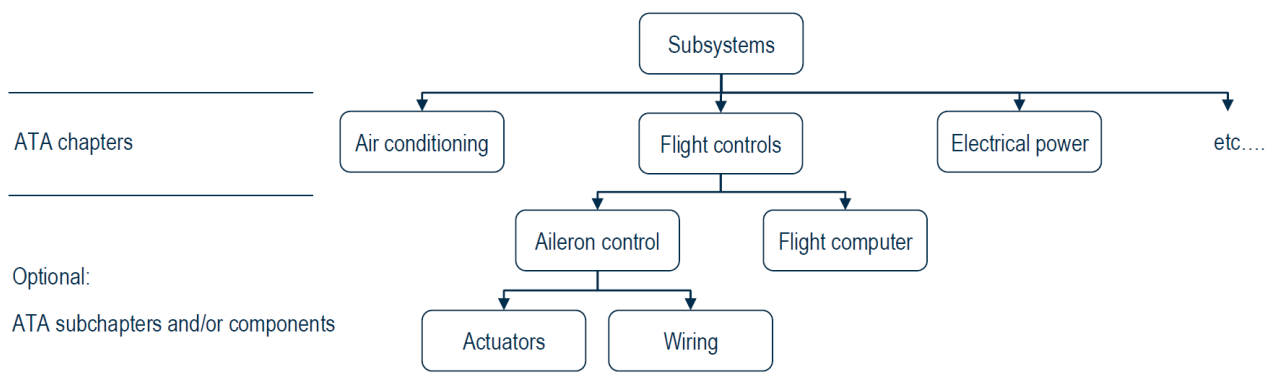

Figure 1: Example of modular subsystems build-up within eFLOWpy.

Table 2: Overview of the ATA chapters considered and their respective power models.

ATA	Name	Power model
21	Air conditioning	Modified method based on Chakraborty [1]
22	Auto flight	ELA value scaled with MTOM
23	Communications	ELA value scaled with MTOM
24	Electrical power	ELA value scaled with MTOM
25	Equipment and furnishings	ELA value scaled with passenger number and base percentage; full galley peak load at beginning of climb and middle of cruise
26	Fire protection	ELA value scaled with MTOM
27	Flight controls	Airbus A320 results of Rao [4] scaled with wing area and flight phase
28	Fuel	ELA value scaled with MTOM
30	Ice and rain protection	Method of Meier [8] with ELA value as constant and de-icing envelope [9]
31	Indicating and recording systems	ELA value scaled with MTOM
32	Landing gear	MRT7-3 results of Li [10] scaled with landing gear mass
33	Lights	ELA value scaled with MTOM
34	Navigation	ELA value scaled with MTOM
35	Oxygen	ELA value scaled with passenger number
38	Water and waste	ELA value scaled with passenger number
45	Central maintenance system	ELA value scaled with MTOM
46	Information systems	ELA value scaled with MTOM
52	Doors	ELA value scaled with MTOM
73	Engine fuel and control	ELA value scaled with MTOM
74	Ignition	ELA value scaled with MTOM
76	Engine controls	ELA value scaled with MTOM
77	Engine indicating	ELA value scaled with MTOM
78	Exhaust	Method of Chakraborty [1]
80	Starting	Boeing 787 required start power [11] scaled with maximum engine thrust

24, 25, 31, 34, 45 and 46 are assumed to fully dissipate into heat, and included in the cabin heat balance. While in current aircraft the galley heat generally does not fully dissipate into the cabin due to separate ventilation systems, this is assumed the case for a conservative approach. The heat balance also includes a fixed metabolic heat load of 75W per occupant and 50W per passenger for the in-flight entertainment system. The solar heat load through the windows is calculated using equation (1) and (2):

$$\dot{Q}_{solar} = intensity(altitude)A_{eff} \qquad (1)$$

$$A_{eff} = 0.5\, A_{window} cos(\theta_{incidence})\tau \qquad (2)$$

where A_{eff} is the effective area, A_{window} the total window area of the aircraft, $\theta_{incidence} = 27°$ the incidence angle of the solar rays, and $\tau = 0.8$ the transmissivity of the windows. The solar intensity has been defined as a function of the altitude as provided in MIL-E-38453A [7]. The heat transfer from the cabin to the ambient is calculated using equations (3) to (6):

$$\dot{Q}_{ambient} = U_{overall}A_{ext}(T_{skin} - T_{cabin}) \qquad (3)$$

$$A_{ext} = 0.90 A_{fus} \qquad (4)$$

$$T_{skin} = T_\infty \left(1 + R_c \frac{\gamma - 1}{2} M_\infty^2\right) \qquad (5)$$

$$R_c = 1 - 0.99(1 - Pr^{0.5}) \qquad (6)$$

$U_{overall}$ represents the overall heat transfer coefficient from the cabin interior wall to the fuselage exterior skin, and is set to $0.5 kW/m^2K$. A_{ext} is the external heat transfer area, and assumed to be 90% of the total fuselage area. The skin temperature is assumed to be equal to the recovery temperature and is calculated using a recovery coefficient R_c, which in turn is based on the Prandtl number, Pr [12]. The cabin is set as one zone with a fixed temperature of 24°C, and the cabin wall temperature is assumed equal to that. The ECS controls the cabin air temperature by changing the temperature of the air injected into it, which can be calculated using equation (7):

$$T_{in} = T_{cabin} + \frac{Q_{ECS}}{\dot{m}_{cabin}C_p} \qquad (7)$$

Q_{ecs} is the heat transferred by the ECS to the cabin, and is determined by the overall cabin heat balance. The minimum air mass flow rate of the air is set to 9.439dm³/s; the total value provided by Hunt et al. for a Boeing 767 [13]. Limits have been set for the inlet air temperature. When the minimum mass flow rate results in an inlet temperature exceeding these limits, the inlet temperature is set to the limit and the mass flow rate is increased to meet the required heat transfer to keep the correct cabin temperature. Furthermore, a recirculation of 50% (i.e. the ECS provides 50% of the required cabin air mass flow rate using fresh outside air, and the other 50% is filtered recirculated air) is assumed, also in line with Hunt et

al. [13]. The ambient ram air required by the ECS passes through a diffuser and electric Cabin Air Compressors (CACs) before it enters the air-cycle machines. Following the approach of Chakraborty [1], the outlet pressure of the CACs is set through a pressure differential with respect to the cabin air pressure: 130kPa at sea level, which linearly decreases to 100kPa at 13.7km altitude. In this study, the cabin pressure is a function of flight altitude and follows that of the Boeing 787 given by Nelson [14]. The power required by all the CACs combined is calculated with equations (8) to (11):

$$P_d = \eta_d P_\infty \left(1 + \frac{\gamma - 1}{2} M_\infty^2\right)^{\frac{\gamma}{\gamma - 1}} \qquad (8)$$

$$P_{CAC} = \Pi_{CAC} P_d \rightarrow \Pi_{CAC} = \frac{P_{cabin} + P_{diff}}{P_d} \qquad (9)$$

$$T_{CAC} = T_d \left\{1 + \frac{1}{\eta_{CAC}} \left(\Pi_{CAC}^{\frac{\gamma - 1}{\gamma}} - 1\right)\right\} \qquad (10)$$

$$Power = \frac{\dot{m}_{ECS} C_p (T_{CAC} - T_d)}{\eta_{EM} \eta_{PE}} \qquad (11)$$

In these equations P_d is the pressure after the diffuser, $\eta_d = 0.95$ the efficiency of the diffuser, P_{CAC} the pressure after the CACs, Π_{CAC} the pressure ratio of the CACs, P_{cabin} the cabin pressure and P_{diff} the pressure differential as explained above. T_{CAC} and T_d are the temperature after the CACs and diffuser respectively, while $\eta_{CAC} = 0.85$ is the efficiency of the CACs. $\eta_{EM} = 0.95$ and $\eta_{PE} = 0.95$ are the efficiencies of the electric motor and the power electronics respectively.

2.1.2. ATA27 flight controls

As a first approximation of the power consumption of the electric flight controls, existing results are scaled according to wing area and flight phase. The results used are those of Rao [4], who created a tool for automated wing subsystem sizing and performed a A320 case study by linking it with the conceptual design tool VAMPzero [15] from the German Aerospace Center (DLR). The result was a total flight controls actuators power consumption of 72kW. The eFLOWpy power model scales this value with wing area, and mission phase based on Figure 4.29 and 4.30 presented in the dissertation of Koeppen [16]. The resulting mission segment scaling values can be found in Table 3. Rather than including a mission profile with full control surface deflections, a simpler approach assuming a constant base load of 20% is used. However, the fuel cell system component sizing considers the full flight controls power load, such that the system is able to provide the maximum power load at any time for extended duration.

Table 3: Mission segment flight controls power-scaling values.

Taxi	0.2	Cruise	1.0
Take-off roll	0.4	Descent	1.0
Take-off	0.8	Landing	0.8
Climb	1.0	Landing roll	0.4

2.2. Fuel cell system modelling

The PEM fuel cell system modelling approach utilises zero-dimensional, static and semi-empirical models. This study only considers a simple and basic system, shown in Figure 2, and leaves potential for further optimisation. Examples of possible improvements not yet considered are:

- A turbine at the cathode exhaust for energy recovery.
- Pre-cooling of the cathode inlet with the cathode exhaust to reduce cooling system requirements and/or improve cathode exhaust energy recovery.
- Direct water injection (evaporation cooling) to cool the fuel cell stacks.
- Integration with other ATA chapters (e.g. potable water, galleys heating with waste heat).

Furthermore, it does not consider any redundancy at this point. Rather, it is assumed that in case of failure the starting motors of the engines can act as generators and provide the necessary power. The following major components of the fuel cell system are modelled: fuel cell cells and stacks, stack cooling modules, centrifugal air compressor, humidifier, power electronics, ultracapacitor, ducts, liquid hydrogen tank, Main Heat eXchanger (MHX) and blower.

2.2.1. Fuel cell stacks

The cells within the PEM fuel cell stacks are modelled using a zero-dimensional, static and semi-empirical approach. The theoretical Nernst voltage is calculated using the Nernst equation [17] and a function of the operating temperature and pressure. Multiple losses are calculated and subtracted from the theoretical voltage, and for more information on the specific models and input parameters, we kindly refer to their respective reference. The activation losses and fuel crossover are calculated using the Butler-Volmer equation with internal current density [18], see equation (12). The Ohmic losses are calculated using the Area-Specific Ohmic Resistance (ASR) [19], see equation (13). Additionally the concentration losses are modelled empirically using an exponential equation as provided in [18], see equation (14).
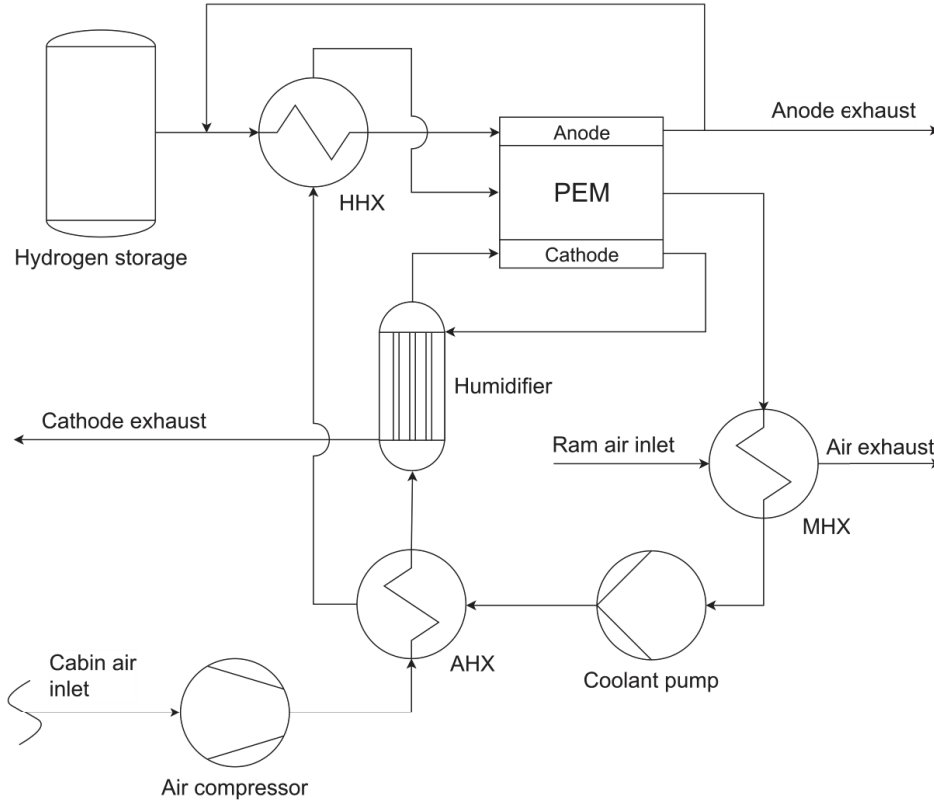
Figure 2: Schematic layout of the fuel cell system considered.

$$\Delta V_{act} = \frac{RT_{op}}{2\alpha F} \ln\left(\frac{i + i_n}{i_0}\right) \qquad (12)$$

$$\Delta V_{Ohm} = i\, ASR_{Ohm} \qquad (13)$$

$$\Delta V_{con} = m \exp(n \cdot i) \qquad (14)$$

Cell degradation over the lifetime of the fuel cell is currently not considered. The efficiency of a fuel cell unit is calculated using equation (15) [18], and based upon the Higher Heating Value (HHV) of hydrogen. The approach does not consider build-up of nitrogen in the fuel cell, caused by recirculation of the unused hydrogen.

$$\eta = \mu_{H_2}\frac{2V_{cell}F}{\Delta \bar{h}_{H_2,HHV}} \qquad (15)$$

An input parameter fitting function ensures the ability to represent state-of-the-art fuel cells with the model. For this work, parameter fitting is performed against a 94kW experimental automotive fuel cell stack resulting from the European AUTOSTACK CORE research project [20]. The experimental fuel cell (Evo2) resulting from this project continued in the commercial PowerCell S3 fuel cell products. Figure 3 shows a comparison between the Evo2 experimental data and the eFLOWpy model output at 68°C and 200kPa. While the model used is relatively simple, it calculates relatively accurate results compared to real fuel cell stacks and is suitable for conceptual design purposes.
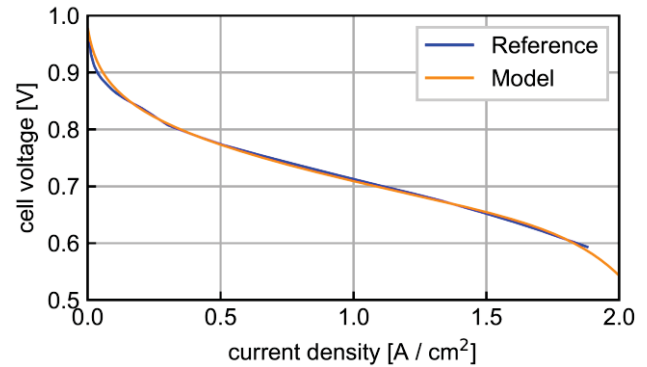

Figure 3: Comparison of the fuel cell stack model input parameter fitting results and the AUTOSTACK CORE Evo2 experimental results [21].

The air and hydrogen mass flow rates are calculated using equations (16) and (17) [18], under the simplifying assumption that all the cells in the stack perform equally.

$$\dot{m}_{air} = 3.57 \cdot 10^{-7}\lambda\frac{P_{stack}}{V_{cell}} \qquad (16)$$

$$\dot{m}_{H_2} = 1.05 \cdot 10^{-8}\frac{P_{stack}}{V_{cell}} \qquad (17)$$

Here λ represents the stoichiometry, which has been set to 2.0 [18]. The heat generated by the stack is calculated using equation (18) [18]:

$$\dot{Q}_{stack} = P_{stack}\left(\frac{1.25}{V_{cell}} - 1\right) \qquad (18)$$

The dedicated model calculates the stack mass and volume through linear regression of the masses and volumes of the different PowerCell S3 stack sizes available [22]. The mass of the stack's cooling module is calculated based on results of the INN-BALANCE project [23], which builds upon the AUTOSTACK CORE project results, and assumes a fixed 1kW power consumption for the coolant pump.

2.2.2. Balance of plant

The balance of plant is modelled with statistical and semi-empirical methods. The major components are modelled individually in terms of mass, volume and power consumption/efficiency. The cylindrical liquid hydrogen tank is sized using a heat transfer analysis that considers both a liquid and gaseous hydrogen state [24]. The centrifugal air compressor is modelled using the approach of Wilson and Korakianitis [25], combined with mass results from Tornabene et al. [26]. The humidifier, power electronics and ultracapacitor properties are scaled from experimental and commercial products [27–30]. The ducts are accounted for using the method described by Hale [31], while the heat exchanger properties are calculated using a standard air cooled finned tube approach [32]. A simple blower scaled from a commercial product [33] has been included, although the power consumption (35-60kW) is not yet integrated within the overall sizing loop.

2.2.3. Aircraft performance

To analyse the effects on aircraft level, the ARB aircraft is modelled in the commercial software package Aircraft Preliminary Design (APD) 3.0 [34]. Within Bauhaus Luftfahrt this tool has been comprehensively supplemented with custom-developed high-end, semi-empirical and analytical methods to allow the design and analysis of both state-of-the-art and future aircraft. For the AVACON study, the change in aircraft block fuel is calculated at different OEMs for the baseline configuration, and a "no off-takes" engine configuration. The latter is implemented by scaling the engine fuel consumption per mid-cruise performance at FL370, M=0.83 and International Standard Atmosphere (ISA) conditions. While this scaling approach will not be accurate at non-cruise conditions, it is deemed acceptable for now as the major part of the mission is flown in cruise conditions. This first assessment also ignores any drag changes, although drag is expected to increase due to the ram air required for the fuel cell cooling system.

3. RESULTS AND DISCUSSION

Figure 4 shows the calculated subsystem power consumptions during the actual mission (not a "worst-case" scenario for each individual subsystem). The mission itself takes place at standard ISA conditions. The top line represents the total power consumption, which peaks just over 350kW during the diversion part of this mission. The largest power consumer is the ECS, which peaks at the end of cruise. The second largest power consumer is the engine starting with close to 150kW, albeit for a short amount of time. One can clearly recognise the anti-ice system cyclic mode from the peaks close to the beginning and end of the mission. The straight line marked by the squares is the flight control system, and does not show any changes throughout each flight segment due to the chosen approach. The related large changes in power consumption, e.g. extension of the flaps, are therefore not included in the results. The total power consumption, however, is not peaking at the time occurrence flap extension would take place. It is therefore not expected that the flap extension will change the maximum peak load occurring during this mission.

A fuel cell sizing point is set to analyse the overall performance on aircraft level. In order to stay close to the reference fuel cell stack properties, a stack power of 100kW is chosen together with an output design power of 500kW. The latter is based on the subsystem power consumption results, and ensures that the system is able to provide enough power to the Flight Control System (FCS) if it were to operate under maximum power requirements. The number of stacks is set to six, such that 100kW remains for operation of the balance of plant. The operating temperature is set to 80°C and therefore within the operating limits of the reference fuel cell [22]. The fuel cell inlet pressures have been set to a sea level pressure of 101kPa. Increasing the pressure to 2bar showed a small increase in performance, but it would also make the system more complex. As this study does not consider full system optimisation yet, it was decided to keep the sea level pressure. The ultracapacitor is sized for 38kW with a 10 seconds discharge time, such that it is able to coop with the anti-icing cyclic peaks while providing the fuel cell system enough time to ramp up. The hydrogen tank was set to a diameter of 1.5m (close to the expected cargo hold height), with 5cm thick insulation. Additionally, 50m of high-pressure ducting provides the possibility for a duct from the wing root to the tail cone of the aircraft for extra integration flexibility.

Table 4 shows the overall fuel cell system results. With a total mass of 1565kg, it is significantly heavier than the ARB Auxiliary Power Unit (APU) dry mass of
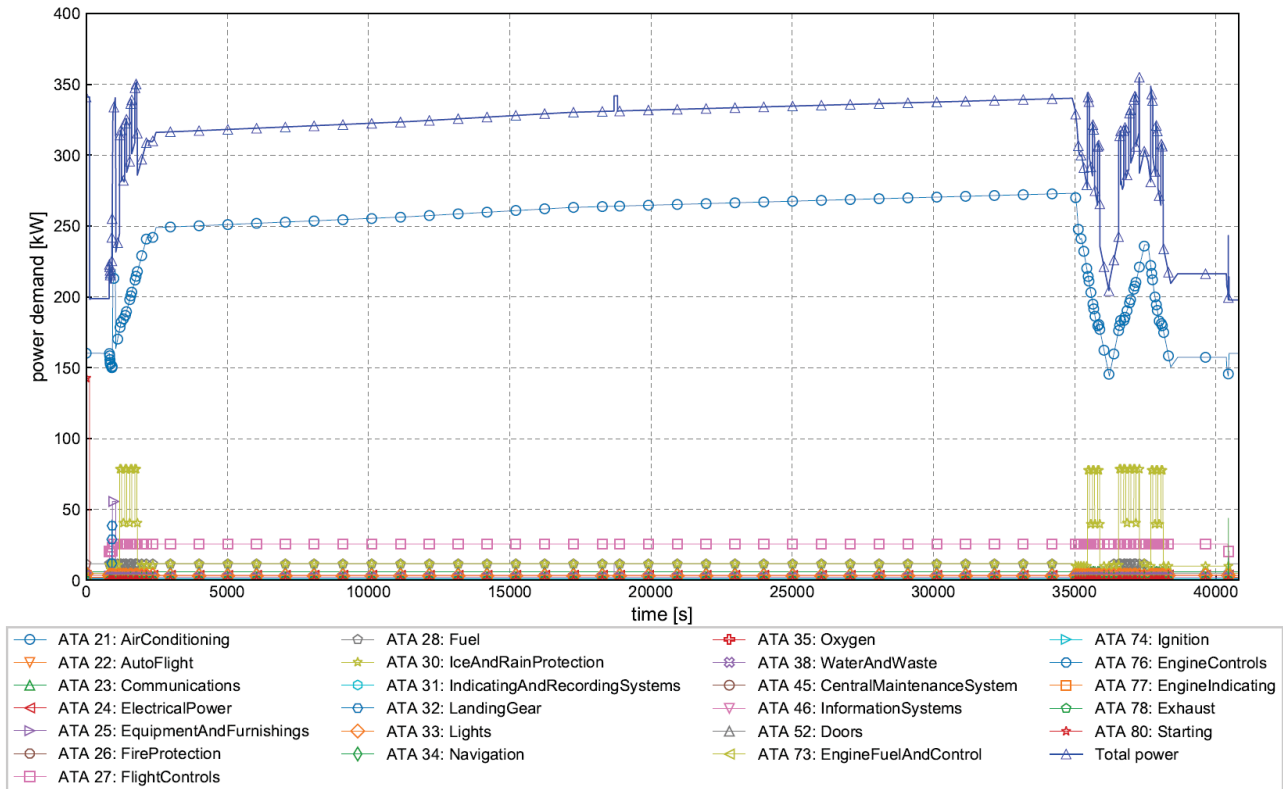
Figure 4: ATA chapters power demand over the mission

309kg. The total mass difference is 1256kg, which excludes the masses of the fuel cell cooling liquid mass and APU related systems that can be removed from the aircraft as well. Based on the outer dimensions provided in [35], the APU volume is estimated to be around 930dm^3. As such, the fuel cell system without hydrogen tank is not much larger and a more efficient cooling system could potentially even result in a smaller system.

Table 4: Fuel cell system mass and volume

Dry fuel cell system mass	1317kg
Liquid hydrogen mass	248kg
Fuel cell system volume	1310dm^3
Hydrogen tank volume	4936dm^3

Table 5 shows the masses and volumes of each of the fuel cell system components. A large portion of the mass is attributed to the cooling system; especially the heat exchanger is relatively heavy and takes up a significant amount of space. As such, it is worthwhile to look at an improved cooling system during fuel cell system optimisation studies. The hydrogen tank size results in a length of 1.27m; i.e. a spherical tank with a diameter of around 1.4m would be optimal in this case taking into consideration structural aspects. An LD3 container has a length of 1.53m by a width of 1.62m. As such, integration of the hydrogen tank within the cargo hold will result in a capacity loss of one LD3 container. In the best scenario, the tank would fit together with the fuel cell

system in the tail cone although more analysis is required on this in terms of available space and centre of gravity shifts.

Table 5: Fuel cell system components mass and volume

Component	Mass [kg]	Volume [dm^3]
Stacks	282	242
Stack cooling modules	110	-
Compressor	16	130
Humidifier	42	78
Power electronics	34	30
Heat exchanger	370	560
Blower	77	200
Ultracapacitor	88	70
Ducts	68	232
Hydrogen tank	230	4936
Liquid hydrogen	248	-

Using the APD results, the total OEM increase of 2883kg combined with the improved performance of the engine without off-takes results in a block fuel saving of 1.2%. This value ignores the energy content of the liquid hydrogen. Although some effects are not yet accounted for (e.g. drag increase, cooling liquid mass, APU systems removal, subsystem synergies), it is expected that including these effects and performing an optimisation of the fuel cell system will yield a 2-3% block fuel reduction. This range is similar to estimations that consider only subsystem

electrification without APU replacement. Hence, on the one hand implementing an APU system increases overall system complexity (both aircraft and ground infrastructure) quite a lot, without additional block fuel benefit. On the other hand, advantages can be expected in terms of noise and emissions during ground operations at airports, especially when electric taxiing can be incorporated as well. As such, it is considered worthwhile to perform optimisation studies to improve the accuracy of the results. Furthermore, solid-oxide fuel cells have the potential to improve the block fuel savings, as they operate at higher temperatures and therefore have lower requirements on the cooling system.

4. CONCLUSIONS AND OUTLOOK

Replacing a conventional APU with a PEM fuel cell system powering a full electric subsystem architecture results in a trade-off between an OEM increase, and an improvement in specific fuel consumption. The results presented in this paper are based on a full mission ATA chapter level power load simulation, and fuel cell system sizing on main component level. They show that a simple PEM fuel cell system results in quite a large OEM increase of more than 1200kg. It is expected that this value can be decreased by performing overall system optimisation, in which the cooling system and utilisation of synergies with other subsystems will play an important role. The results presented here also show that a PEM based fuel cell system will most likely not lead to an improvement in block fuel consumption, compared to a full electric architecture powered by conventional generators. Rather, the benefits are to be sought after in terms of noise and emissions on ground. Follow up work should focus on improving the subsystems models, e.g. FCS, as well as optimisation of the PEM fuel cell system. Additionally it can be worthwhile to investigate of SOFC fuel cells have a better potential to reduce mission block fuel, since their heat management requirements are lower. In the near future SOFC fuel cell systems will be added to eFLOWpy to perform such investigations.

Contact:
Jasper.vanWensveen@bauhaus-luftfahrt.net

REFERENCES

[1] Chakraborty, I., "Subsystem architecture sizing and analysis for aircraft conceptual design", Dissertation, *Daniel Guggenheim School of Aerospace Engineering,* Georgia Institute of Technology, 2015.

[2] Tagge, G. E., Irish, L. A., and Bailey, A. R., "Systems study for an Integrated Digital-Electric Aircraft (IDEA)", NASA Contractor Report 3840, 1985, URL: https://ntrs.nasa.gov/search.jsp?R=19850007405 [retrieved 29 November 2019].

[3] Jones, R. I., "The more electric aircraft—assessing the benefits" *Proceedings of the Institution of Mechanical Engineers, Part G: Journal of Aerospace Engineering*, Vol. 216, No. 5, 2002, pp. 259–269. doi: 10.1243/095441002321028775

[4] Rao, N. K., "Influence of Parametric Modelling of Wing Subsystems on the Aircraft Design and Performance", Master's dissertation, *Faculty of Aerospace Engineering,* Delft University of Technology, Delft, 2017.

[5] Jomier, T., "More Open Electrical Technologies (MOET) deliverable D0.02.3: Technical Report", 2009, URL: https://trimis.ec.europa.eu/project/more-open-electrical-technologies [retrieved 29 November 2019].

[6] BOGGERO, L., "Design techniques to support aircraft systems development in a collaborative MDO environment", Dissertation, Politecnico di Torino, Turin, 2018.

[7] United States Air Force, "MIL-E-38453A Environmental Control, Environmental Protection, and Engine Bleed Air Systems, Aircraft, General Specification for", 1971.

[8] Meier, O. and Scholz, D., "A handbook method for the estimation of power requirements for electrical de-icing systems", Deutscher Luft- und Raumfahrt Kongress 2010, Hamburg, Germany, August 31 - September 2, 2010.

[9] European Union Aviation Safety Agency, "Certification Specifications and Acceptable Means of Compliance for Large Aeroplanes CS-25". Amendment 23, 15 Jul 2019, URL: https://www.easa.europa.eu/document-library/certification-specifications/cs-25-amendment-23 [retrieved 29 November 2019].

[10] Li, W. and Fielding, J. P., "Preliminary study of EMA landing gear actuation", 28th Congress of the International Council of the Aeronautical Sciences, Brisbane, Australia, September 23-28, 2012.

[11] Boeing Commercial Airplanes, "787 Airplane Characteristics for Airport Planning", 2018 [retrieved 29 November 2019].

[12] SAE, "AIR1168/3: Aerothermodynamic Systems Engineering and Design", 2011.

[13] Hunt, E. H., Reid, D. H., Space, D. R., and Tilton, F. E., "Commercial Airliner Environmental Control System: Engineering Aspects of Cabin Air Quality", Aerospace Medical Association annual meeting, Anaheim, California, May, 1995.

[14] Nelson, T., "787 Systems and Performance", 2005, URL: http://myhres.com/Boeing-787-Systems-and-Performance.pdf [retrieved 31 October 2019].

[15] Bohnke, D., Nagel, B., and Gollnick, V., "An approach to multi-fidelity in conceptual aircraft design in distributed design environments", 2011 IEEE Aerospace Conference, Big Sky, USA, March 5-12, 2011. doi: 10.1109/AERO.2011.5747542

[16] Koeppen, C., *Methodik zur modellbasierten Prognose von Flugzeugsystemparametern im Vorentwurf von Verkehrsflugzeugen,* Shaker Verlag, Aachen, Germany, 2006, ISBN: 978-3-8322-5234-2.

[17] Gao, F., Blunier, B., and Miraoui, A., *Proton Exchange Membrane Fuel Cells Modeling,* John Wiley & Sons, Inc, Hoboken, NJ USA, 2012, ISBN: 9781118562079.

[18] Larminie, J. and Dicks, A., *Fuel Cell Systems Explained,* John Wiley & Sons, Ltd, West Sussex, England, 2003, ISBN: 9781118878330.

[19] Spiegel, C., *PEM Fuel Cell Modeling and Simulation Using Matlab,* Elsevier, 2008, ISBN: 9780123742599.

[20] Jörissen, L., "Auto-Stack CORE: A Summery", 2013, URL: http://autostack.zsw-bw.de/fileadmin/public_information/docs/CORE/130708_Auto-Stack_CORE_general_external.pdf [retrieved 22 November 2019].

[21] Jörissen, L., "AutoStack-CORE Automotive Fuel Cell Cluster for Europe II: Programme Review Days 2017", 2017, URL: https://www.fch.europa.eu/sites/default/files/S2_P2_Pres6_JOERISSEN_AUTO-STACK%20CORE%20%28ID%202909951%29.pdf [retrieved 28 November 2019].

[22] PowerCell, "PowerCell S3: 30-125 kW PEM technology", 2018, URL: https://www.powercell.se/wordpress/wp-content/uploads/2018/12/powercell-s3-datasheet-pdf-190129.pdf [retrieved 6 November 2019].

[23] Haberl, F., "Deliverable 1.4: Public results of the architecture and system level optimization", 2018, URL: https://www.innbalance-fch-project.eu/fileadmin/user_upload/downloads/D1.4_submitted.pdf [retrieved 6 November 2019].

[24] Gradwohl, G., "Conceptual Design of a Fuel Cell Powered All Electric Regional Aircraft", Diploma thesis, FH Joanneum, 2011.

[25] Wilson, D. G. and Korakianitis, T., *The design of high-efficiency turbomachinery and gas turbines,* MIT, Cambridge, Massachusetts and London, England, 2014, ISBN: 9780262526685.

[26] Tornabene, R., Wang, X.-y., Steffen, C. J., and Freeh, J. E., "Development of Parametric Mass and Volume Models for an Aerospace SOFC/Gas Turbine Hybrid System", NASA/TM-2005-213819, 2005, URL: https://ntrs.nasa.gov/search.jsp?R=2005020384 [retrieved 6 November 2019].

[27] fumatech, "Membrame Humidifiers: fumasep® High Performance Membrane Humidifiers for Fuel Cells", URL: https://www.fumatech.com/NR/rdonlyres/0B9A1C7F-5BA6-4409-A003-5C4E79CD61AB/0/FUMATECH_BWT_GmbHMembrane_Humidifiers.pdf [retrieved 6 November 2019].

[28] Faunhofer IISB, "Bidirectional full SiC 200 kW DC-DC Converter for Electric, Hybrid and Fuel Cell Vehicles", 2015, URL: https://www.mikroelektronik.fraunhofer.de/content/dam/mikroelektronik/Datenbltter/IISB_200kW-Rekordwandler_DB.pdf [retrieved 6 November 2019].

[29] Yin, S., Tseng, K. J., Simanjorang, R., Liu, Y., and Pou, J., "A 50-kW High-Frequency and High-Efficiency SiC Voltage Source Inverter for More Electric Aircraft" *IEEE Transactions on Industrial Electronics*, Vol. 64, No. 11, 2017, pp. 9124–9134. doi: 10.1109/TIE.2017.2696490

[30] Maxwell Technologies, "Datasheet: 3.0V 3400F ULTRACAPACITOR CELL: Maxwell's Highest Power and Energy Cell", 2018, URL: https://www.maxwell.com/images/documents/3V_3400F_datasheet.pdf [retrieved 6 November 2019].

[31] Hale, P. L., "A method to estimate weight and dimensions of small aircraft propulsion gas turbine engines: Final Report and User's Guide", 1982, URL: https://ntrs.nasa.gov/archive/nasa/casi.ntrs.nasa.gov/19830008072.pdf [retrieved 6 November 2019].

[32] Gas Processors Suppliers Association, *Engineering Data Book, Section 10: Air-Cooled Exchangers. FPS Version*, Ed. 12, 2004.

[33] ebm-papst, "Compact fans for AC, DC and EC", 2019, URL: https://www.ebmpapst.com/media/content/info-center/downloads_10/catalogs/compactfansen2011/Compact_fans_for_AC_and_DC_2016_01_US.pdf [retrieved 6 November 2019].

[34] TXT, "Pacelab APD", URL: https://www.txtgroup.com/markets/solutions/pacelab-apd/ [retrieved 6 November 2019].

[35] Scholz, D., "An optional APU for passenger aircraft", 5th *CEAS Air and Space Conference*, Delft, Netherlands, September 7-11, 2015.